Inorg. Chem. **2006**, *45*, 4537−4543

Novel Stoichiometrically Erbium−Ytterbium Cocrystalline Complex Exhibiting Enhanced Near-Infrared Luminescence

Qi Zhong,[†] Huaishan Wang,[†] Guodong Qian,*[,†] Zhiyu Wang,[†] Jiahua Zhang,[‡] Jianrong Qiu,[†] and Minquan Wang[†]

Department of Materials Science & Engineering, State Key Laboratory of Silicon Materials, Zhejiang University, Hangzhou 310027, China, and Key Laboratory of Excited-State Processes, Changchun Institute of Optics, Fine Mechanics and Physics, China Academy of Science, Changchun 130021, China

Received October 1, 2005

Three β-diketonate complexes of erbium and ytterbium, $Er(HFA)_3(TPPO)_3$, $Yb(HFA)_3(TPPO)_3$, and $Er_{1/2}Yb_{1/2}(HFA)_3(TPPO)_2$ (HFA = hexafluoroacetylacetonate, TPPO = triphenylphosphine oxide) are synthesized and structurally characterized, and their luminescent properties are examined in detail. Compared with monometallic complexes $Er(HFA)_3(TPPO)_3$ and $Er(HFA)_3(TPPO)_3$, the stoichiometrically Er−Yb cocrystalline complex $Er_{1/2}Yb_{1/2}(HFA)_3(TPPO)_2$ exhibits special indirect near-infrared (NIR) luminescence with the acceptor and sensitizer (donor) coexisting in a single crystal. Of interest is that the NIR luminescence of the erbium ion in $Er_{1/2}Yb_{1/2}(HFA)_3(TPPO)_2$ is significantly enhanced because of the coexistence of the ytterbium ion through the energy-transfer between the ytterbium and erbium ions. The estimated donor−acceptor energy-transfer critical radii $R_{C,DA}$, obtained from the Förster model, are in good agreement with those determined from the single X-ray crystal structure, confirming the dipole−dipole character for such a Yb−Er energy-transfer process.

Introduction

Erbium organic complexes that possess near-infrared (NIR) luminescence resulting from the $^4I_{13/2} \rightarrow {}^4I_{15/2}$ transition of the central erbium ions are of special interest because of their potential applications in polymer-derived optical amplifiers and organic−inorganic hybrid-derived optical amplifiers operating at 1.54 μm.[1,2] Direct excitation on the Er^{3+} ions at 980 nm is less efficient because of their very low absorption coefficient, while the Yb^{3+} ion has 1 order of magnitude more absorption cross-section at this wavelength than does the Er^{3+} ion. In effect, a usual method to improve the pumping efficiency of Er^{3+} ions is to use a 980 nm semiconductor laser diode (LD) because of the Yb^{3+} ions' higher absorption cross-section. Indirect excitation of the Er^{3+} ions occurs mainly via energy transfer from the $^2F_{5/2}$ level of the Yb^{3+} ion to the $^4I_{11/2}$ level of the Er^{3+} ion. In view of the short lifetime of $^4I_{11/2}$, the energy back-transfer from Er^{3+} to Yb^{3+} is negligible at the same time. An erbium-doped glass host codoped with ytterbium has already been implemented in optical fiber amplifiers, and the energy-transfer process between Er^{3+} and Yb^{3+} has also been demonstrated.[2−5] Nevertheless, most work related to erbium organic complexes has been focused on monometallic erbium complexes and

* To whom correspondence should be addressed. E-mail: gdqian@zju.edu.cn.
[†] Zhejiang University.
[‡] Changchun Institute of Optics, Fine Mechanics and Physics.

(1) (a) Polman, A.; Veggel, F. C. J. M. V. *J. Opt. Soc. Am. B* **2004**, *21*, 871−892. (b) Slooff, L. H.; Blaaderen, A. V.; Polman, A.; Hebbink, G. A.; Klink, S. I.; Veggel, F. C. J. M. V.; Reinhoudt, D. N.; Hofstraat, J. W. *J. Appl. Phys.* **2002**, *91*, 3955−3980. (c) Polman, A. *Proc. SPIE−Int. Soc. Opt. Eng.* **2000**, *3942*, 1−12. (d) Slooff, L. H.; Polman, A.; Wolbers, M. P. O.; Veggel, F. C. J. M. V.; Reinhoudt, D. N.; Hofstraat, J. W. *J. Appl. Phys.* **1998**, *83*, 497−503.

(2) Wong, W. H.; Pun, E. Y. B.; Chan, K. S. *Appl. Phys. Lett.* **2004**, *84*, 176−178.

(3) (a) Jones, D. J.; Namiki, S.; Ippen, E. P.; Haus, H. A.; Barbier, D. In *Proceedings of the Optical Fiber Communication Conference and Exhibit*; OFC '98, San Jose, CA; Optical Society of America: Washington, DC, 1998; pp 371−372. (b) Barbier, D.; Bruno, P.; Cassagnettes, C.; Trouillon, M.; Hyde, R. L.; Kevorkian, A.; Delavaux, J. M. P. In *Proceedings of the Optical Fiber Communication Conference and Exhibit*; OFC '98, San Jose, CA: Optical Society of America: Washington, DC, 1998; pp 45−46. (c) Wong, E. M. W.; Man, S. Q.; Pun, E. Y. B.; Chung, P. S. In *Proceedings of the 1999 IEEE Hong Kong Electron Devices Meeting*; Institute of Electrical and Electronics Engineers: New York, 1999; pp 26−29.

(4) (a) Obaton, A.-F.; Parent, C.; Flem, G. L.; Thony, P.; Brenier, A.; Boulonc, G. *J. Alloys Compd.* **2000**, *300−301*, 123−130. (b) Veasey, D. L.; Funk, D. S.; Peters, P. M.; Sanford, N. A.; Obarski, G. E. *J. Non-Cryst. Solids* **2000**, *263−264*, 369−381. (c) Hu, Y.; Jiang, S.; Luo, T.; Seneschal, K.; Morrell, M.; Smektala, F.; Honkanen, S.; Lucas, J.; Peyghambarian, N. *IEEE Photonics Technol. Lett.* **2001**, *13*, 657−659.

10.1021/ic051697y CCC: $33.50
Published on Web 05/03/2006

the sensitization of Er^{3+} luminescence at 1.54 μm by organic ligands,[6,7] which cannot utilize the cheap semiconductor LD as the excitation source since the maximum absorption bands of organic ligands are usually in the ultraviolet or visible region. There has been very little work on mixed lanthanide complexes for their near-infrared luminescence.[8] Herein we report a stoichiometrically Er−Yb cocrystalline complex, $Er_{1/2}Yb_{1/2}(HFA)_3(TPPO)_2$ (HFA = hexafluoroacetylacetonate, TPPO = triphenylphosphine oxide) exhibiting indirect near-infrared (NIR) luminescence with the acceptor and sensitizer (donor) coexisting in a single crystal and an enhanced NIR luminescence of the erbium ion through energy transfer between the ytterbium and erbium ions.

Experimental Section

Synthesis and Characterization of Complexes. All reagents, including hexafluoroacetylacetone (H-HFA), triphenylphosphine oxide (TPPO), Er_2O_3, and Yb_2O_3, were reagent grade and used as received. $ErCl_3{\cdot}6H_2O$ or $YbCl_3{\cdot}6H_2O$ was obtained from Er_2O_3 or Yb_2O_3 by dissolution in hydrochloric acid and the subsequent careful removal of the the solvent. Monometallic organic complexes and the Er−Yb cocrystalline organic complex, $Ln(HFA)_3(TPPO)_2$ (Ln = Er, Yb, or $Er_{1/2}Yb_{1/2}$), were synthesized through the general procedure described in the ref 9, confirmed by elemental analysis and FTIR. Here, the procedure for the preparation of $Er_{1/2}Yb_{1/2}(HFA)_3(TPPO)_2$ was described as an example. Ten milliliter aqueous solutions of 1 mmol $ErCl_3{\cdot}6H_2O$ and 1 mmol $YbCl_3{\cdot}6H_2O$ were added to a solution of 6 mmol of H-HFA and 6 mmol of KOH in 50 mL of ethanol and 50 mL of water, followed by the addition of 4 mmol of TPPO. The mixture was allowed to stand overnight at room temperature, after which the solvent was concentrated in an oven, and the crystalline product was collected on a filter, washed with water, and dried in vacuo. Hereafter, the ethanol solution of the dried crystalline product was stored in a sealed flask at room temperature for half of a month; then, the single-crystal product, suitable for X-ray analysis, was collected by filtration.

Table 1. Crystal Data Collection and Refinement Details for the Crystal Structure of $Er(HFA)_3((TPPO)_2$

empirical formula	$C_{51}H_{30}O_8P_2F_{18}Er$
fw	1341.97
cryst syst	monoclinic
space group	$P2_1/n$
a (Å)	17.4229(5)
b (Å)	15.5910(3)
c (Å)	20.5218(8)
β (deg)	93.4940(8)
V (Å^3)	5564.2(3)
Z	4
D_{calcd} (g/cm^3)	1.602
μ (cm^{-1})	16.73
temp (K)	298
F(000)	2640
measured reflns	47 260
unique reflns	12 285 [R_{int}=0.056]
reflns with $I > 2\sigma(I)$	7272
refined params	721
R1[a]$(I>2\sigma(I))$	0.040
wR2[b]$(I>2\sigma(I))$	0.094

[a] $R1 = \sum||F_o| - |F_c||/\sum|F_o|$. [b] $wR2 = [\sum w(F_o^2 - F_c^2)/\sum w(F_o^2)^2]^{1/2}$.

All three complexes were characterized by FTIR (Nicolet Avatar 360 FTIR), elemental analysis (CE Instruments Eager 200), and thermal analysis. Anal. Calcd for $Er(HFA)_3(TPPO)_2$: C, 45.60; H, 2.25. Found: C, 45.98; H, 2.65. Anal. Calcd for $Er_{1/2}Yb_{1/2}(HFA)_3(TPPO)_2$: C, 45.55; H, 2.23. Found: C, 45.57; H, 2.54. Anal. Calcd for $Yb(HFA)_3(TPPO)_2$: C, 45.40; H, 2.21. Found: C, 45.78; H, 2.48. FTIR and TG-DSC data are attached in the Supporting Information (Figures S1 and S2).

X-ray Crystallographic Study. A single crystal of $Er(HFA)_3(TPPO)_2$ suitable for X-ray analysis was mounted on a glass fiber. Data were collected at 20 °C on a Rigaku RAXIS RAPID imaging plate area detector with graphite-monochromated Mo Kα radiation. Of the 47 260 reflections that were collected, 12 285 were unique (R_{int} = 0.056), and the equivalent reflections were merged. The structure was solved by and expanded using Fourier techniques.[10] Lattice and data collection parameters are summarized in Table 1. All calculations were performed using the CrystalStructure crystallographic software package (CrystalStructure 3.6.0: Crystal Structure Analysis Package, Rigaku and Rigaku/MSC (2000−2004), 9009 New Trails Dr., The Woodlands, TX 77381). Non-hydrogen atoms were refined anisotropically and hydrogen atoms were refined using the riding model. The final cycle of full-matrix least-squares refinement on F^2 was based on 7272 observed reflections and 751 variable parameters.

Photophysical Measurement. Ultraviolet−visible near-infrared (UV−Vis NIR) absorption spectra were recorded on a Perkin-Elmer Lambda 20 spectrometer at a spectral resolution of 1 nm. Steady-state photoluminescence (PL) measurements in the NIR region were performed at room temperature using a TRIAX 550 spectrometer equipped with a thermoelectric-cooled InGaAs detector (DSS−IGA020T, JOBIN YVON/SPEX) and with 355 nm third harmonic light of a pulsed Nd:YAG laser or a 980 nm LD as the excitation source. The spectral resolution and the integral time were 2 nm and 1 s, respectively, for all PL measurements. Time-dependent luminescence spectra were obtained by measuring the growth and decay of the luminescence intensity at a series of wavelengths. The growth and decay spectra of the luminescence intensity for the excited Yb^{3+} ion or the Er^{3+} ion at selected wavelengths were

(5) (a) Chryssou, C. E.; Di Pasquale, F.; Pitt, C. W. *J. Lightwave Technol.* **2001**, *19*, 345−349. (b) Chen, H. Y.; Liu, Y. Z.; Dai, J. Z.; Yang, Y. P.; Guan, Z. G.; Huang, X. L. In *Communications, Circuits and Systems and West Sino Expositions*; Proceedings of the IEEE 2002 International Conference on Image Processing; Institute of Electrical and Electronics Engineers: Washington, DC, 2002; Vol. 1, pp 827−829. (c) Chiasera, A.; Tosello, C.; Moser, E.; Montagna, M.; Belli, R.; Goncalves, R. R.; Righini, G. C.; Pelli, S.; Chiappini, A.; Zampedri, L.; Ferrari, M. *J. Non-Cryst. Solids* **2003**, *322*, 289−294.

(6) (a) Steemers, F. J.; Verboom, W.; Hofstraat, J. W.; Geurts, F. A. J.; Reinhoudt, D. N. *Tetrahedron Lett.* **1998**, *39*, 7583−7586. (b) Brandell, D.; Klintenberg, A. M.; Aablooc, A.; Thomas, J. O. *J. Mater. Chem.* **2002**, *12*, 565−569. (c) Destri, S.; Porzio, W.; Meinardi, F.; Tubino, R.; Salerno, G. *Macromolecules* **2003**, *36*, 273−275.

(7) (a) Deun, R. V.; Fias, P.; Driesen, K.; Binnemans, K.; Görller-Walrand, C. *Phys. Chem. Chem. Phys.* **2003**, *5*, 2754−2757. (b) Park, O.-H.; Seo, S.-Y.; Bae, B.-S.; Shin, J. H. *Appl. Phys. Lett.* **2003**, *82*, 2787−2789. (c) Suzuki, H.; Hattori, Y.; Iizuka, T.; Yuzawa, K.; Matsumoto, N. *Thin Solid Films* **2003**, *438−439*, 288−293. (d) Pizzoferrato, R.; Lagonigro, L.; Ziller, T.; Di Carlo, A.; Paolesse, R.; Mandoj, F.; Ricci, A.; Lo Sterzo, C. *Chem. Phys.* **2004**, *300*, 217−225.

(8) (a) Wong, W.-K.; Hou, A.; Guo, J.; He, H.; Zhang, L.; Wong, W.-Y.; Li, K.-F.; Cheah, K.-W.; Xue, F.; Mak, T. C. W. *J. Chem. Soc., Dalton Trans.* **2001**, 3092−3098. (b) Goncülves e Silva, F. R.; Malta, O. L.; Reinhard, C.; Güdel, H.-U.; Piguet, C.; Moser, J. E.; Bünzli, J.-C. G. *J. Phys. Chem. A* **2002**, *106*, 1670−1677. (c) Bassett, A. P.; Magennis, S. W.; Glover, P. B.; Lewis, D. J.; Spencer, N.; Parsons, S.; Williams, R. M.; De Cola, L.; Pikramenou, Z. *J. Am. Chem. Soc.* **2004**, *126*, 9413−9424.

(9) Wang, H.; Qian, G.; Wang, Z.; Zhang, J.; Luo, Y.; Wang, M. *J. Lumin.* **2005**, *113*, 214−220.

(10) Beurskens, P. T.; Admiraal, G.; Beurskens, G.; Bosman, W. P.; de Gelder, R.; Israel, R.; Smits, J. M. M. *Technical Report of the Crystallography Laboratory*; University of Nijmegen: Nijmegen, Netherlands, 1999.

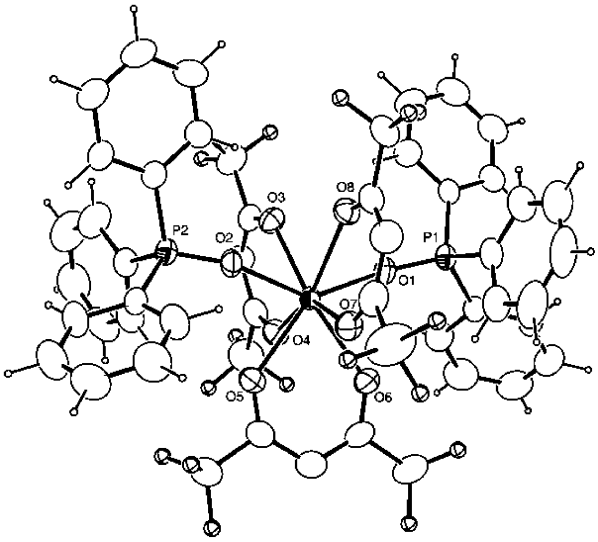

Figure 1. ORTEP drawing of $Er(HFA)_3(TPPO)_2$. Three hydrogen atoms in the HFA ligands have been omitted for clarity.

Chart 1. Chemical Structures for the Molecular Formulas $Ln(HFA)_3((TPPO)_2$ (Ln = Er, Yb, or $Er_{1/2}Yb_{1/2}$)

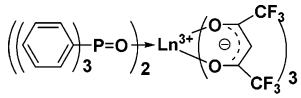

$Ln(HFA)_3(TPPO)_2$ Ln= Er, Yb or $Er_{1/2}Yb_{1/2}$

determined by monitoring the luminescence decay after excitation with a 10 ns pulse and 20 Hz repetition rate of a third-harmonized Nd:YAG laser, detected using the InGaAs detector and recorded with a digital oscilloscope (TDS3052, Tektronix). Luminescence lifetimes were obtained by deconvolution of the measured detector response with monoexponential components for growth and decay of lanthanide ion luminescence.

Results and Discussion

Stoichiometry and Crystal Structures. The compositions of the three complexes were confirmed by elemental analysis, together with powder X-ray diffraction studies. The stoichiometry of the Er−Yb cocrystalline complex, $Er_{1/2}Yb_{1/2}(HFA)_3(TPPO)_2$, was further confirmed by EDS analysis (Oxford RNCA) with Er and Yb weight percentages of 11.77 and 11.28%, respectively, indicating a 1:1 molar ratio of Er/Yb (see Figure S3 and Table S1 in the Supporting Information). Powder X-ray diffraction studies showed that they are isostructural, and the single X-ray crystal structure of $Er(HFA)_3(TPPO)_2$ was characterized. Their illustrated chemical structures are shown in Chart 1, and the single X-ray molecular structure of $Er(HFA)_3(TPPO)_2$ is shown in Figure 1; detailed crystallographic data is presented in Table 1. The structure of the $Er(HFA)_3(TPPO)_2$ molecule consists of an erbium ion which is coordinated by six oxygen atoms of three bidentate HFA ligands and two oxygen atoms of two monodentate TPPO. The symmetry around the erbium ion is approximately square antiprismatic. Er−O(HFA) and Er−O(TPPO) bond distances are comparable to those found in similar Er compounds.[11,12]

There are four $Er(HFA)_3(TPPO)_2$ molecules in each unit cell, which are packed by intermolecular van der Waals interactions and $\pi-\pi$ interactions from benzenes of different

Table 2. Selected Bond Lengths (Å) and Angles (deg) for the Crystal Structure of $Er(HFA)_3((TPPO)_2$[a]

Er(1)−O(1)	2.235(4)	Er(1)−O(2)	2.240(4)
Er(1)−O(3)	2.393(4)	Er(1)−O(4)	2.293(4)
Er(1)−O(5)	2.350(4)	Er(1)−O(6)	2.356(4)
Er(1)−O(7)	2.315(4)	Er(1)−O(8)	2.360(4)
Er(1)−O(1)−P(1)	155.1(2)	O(2)−Er(1)−O(1)	142.8(1)
O(3)−Er(1)−O(1)	77.9(1)	O(4)−Er(1)−O(1)	85.3(1)
O(5)−Er(1)−O(1)	143.2(1)	O(6)−Er(1)−O(1)	73.2(1)
O(7)−Er(1)−O(1)	105.1(1)	O(8)−Er(1)−O(1)	73.7(1)
Er(1)−O(2)−P(2)	156.3(2)	O(3)−Er(1)−O(2)	73.0(1)
O(4)−Er(1)−O(2)	106.5(1)	O(5)−Er(1)−O(2)	73.5(1)
O(6)−Er(1)−O(2)	143.3(1)	O(7)−Er(1)−O(2)	86.4(1)
O(8)−Er(1)−O(2)	76.5(1)	O(4)−Er(1)−O(3)	71.7(1)
O(5)−Er(1)−O(3)	121.9(1)	O(6)−Er(1)−O(3)	138.7(1)
O(7)−Er(1)−O(3)	144.2(1)	O(8)−Er(1)−O(3)	74.5(1)
Er(1)−O(3)−C(37)	134.7(4)	O(5)−Er(1)−O(4)	74.2(1)
O(6)−Er(1)−O(4)	77.1(1)	O(7)−Er(1)−O(4)	143.6(1)
O(8)−Er(1)−O(4)	143.1(1)	Er(1)−O(4)−C(39)	136.8(4)
O(6)−Er(1)−O(5)	72.5(1)	O(7)−Er(1)−O(5)	77.3(1)
O(8)−Er(1)−O(5)	138.2(1)	Er(1)−O(5)−C(42)	134.9(4)
O(7)−Er(1)−O(6)	73.1(1)	O(8)−Er(1)−O(6)	122.9(1)
Er(1)−O(6)−C(44)	134.9(4)	O(8)−Er(1)−O(7)	72.4(1)
Er(1)−O(7)−C(47)	135.7(4)	Er(1)−O(8)−C(49)	134.0(4)

[a] Symmetry transformations used to generate equivalent atoms: (#1) $-x + 1/2, y + 1/2, -z + 1/2$; (#2) $x + 1/2 - 1, -y + 1/2, z + 1/2 - 1$; (#3) $-x, -y + 1, -z + 1$; (#4) $x + 1/2, -y + 1/2, z + 1/2 - 1$; (#5) $-x + 1, -y + 1, -z + 1$.

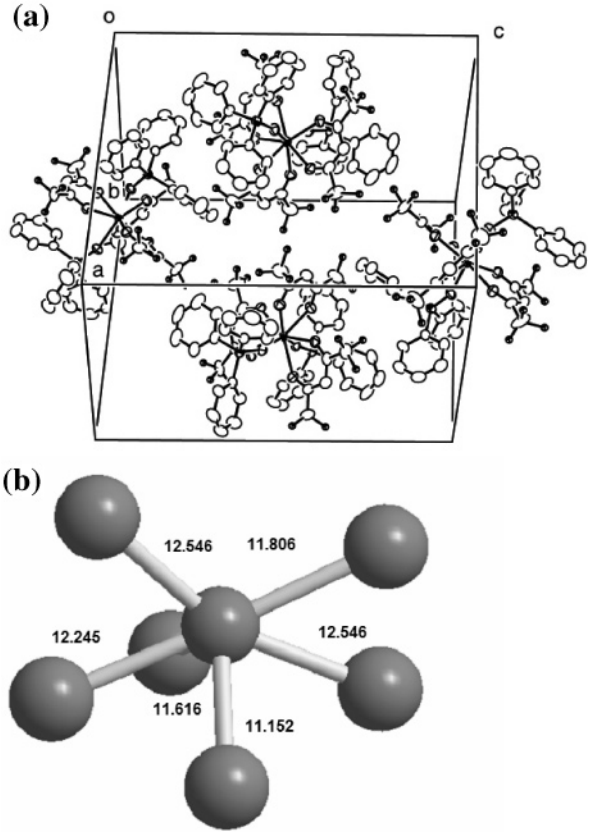

Figure 2. (a) Unit cell packing structure of $Er(HFA)_3(TPPO)_2$, (b) the corresponding schematic illustration indicating the intermolecular $Er^{3+}\cdots Er^{3+}$ distances (Å) between one metal site and its six neighboring sites, and the schematic illustration of the six neighboring metal sites revealed in the molecular packing of $Er(HFA)_3(TPPO)_2$.

molecules (Figure 2a). We paid close attention to the intermolecular $Ln^{3+}\cdots Ln^{3+}$ distances which play significant roles in their NIR luminescent properties. The molecular packing indicates that there are six representative intermo-

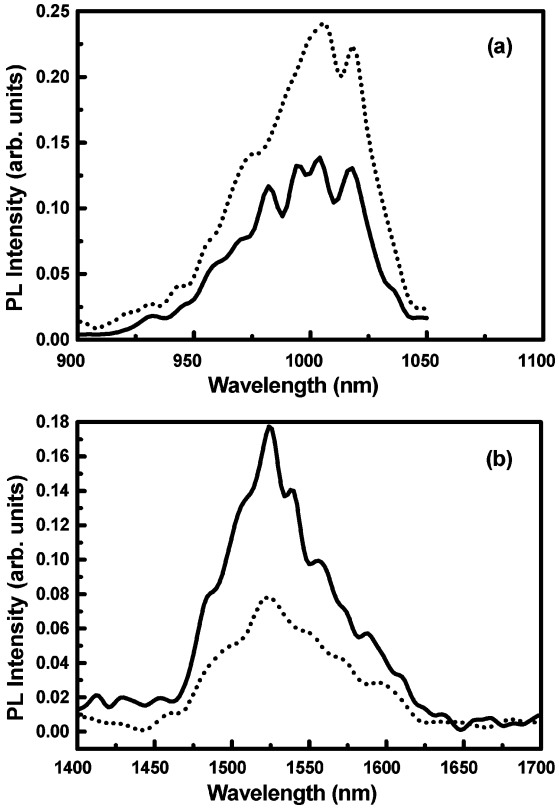

Figure 3. (a) NIR PL spectra of $Er_{1/2}Yb_{1/2}(HFA)_3(TPPO)_2$ (solid line) and $Yb(HFA)_3(TPPO)_2$ (dotted line) around 1000 nm and (b) the NIR PL spectrum of $Er_{1/2}Yb_{1/2}(HFA)_3(TPPO)_2$ (solid line) and $Er(HFA)_3(TPPO)_2$ (dotted line) around 1500 nm. The bulky microcrystalline powder was excited at 355 nm by a Nd:YAG laser at room temperature.

lecular $Er^{3+}\cdots Er^{3+}$ distances of around 10, 11.152, 11.616, 11.806, 12.245, 12.546, and 12.546 Å (Figure 2b). As the Er−Yb cocrystalline complex, $Er_{1/2}Yb_{1/2}(HFA)_3(TPPO)_2$, is isostructural with $Er(HFA)_3(TPPO)_2$, it is reasonably assumed that the intermolecular $Er^{3+}\cdots Yb^{3+}$ distances in $Er_{1/2}Yb_{1/2}$-$(HFA)_3(TPPO)_2$ are in the same order.

Other important distances which may affect the NIR luminescence properties are the intramolecular distances between the lanthanide ion and the hydrogen atom from adjacent C−H oscillators, which are listed in Table S2 of the Supporting Information for complex $Er(HFA)_3(TPPO)_2$. It has been known that C−H units will cause luminescence quenching if the hydrogen atoms are close to the luminescent lanthanide ion ($H\cdots Ln^{3+}$ distances within 6 Å);[13] thus three C−H units in the three HFA β-diketonate ligands ($H\cdots Er^{3+}$ distances of 4.81∼4.83 Å) and ten C−H units from two TPPO ligands will contribute to the luminescence quenching, leading to a decrease of the quantum yield in their complexes.

Photophysical Properties and Energy-Transfer Process. Figure 3a shows q NIR PL spectrum of $Yb(HFA)_3(TPPO)_2$ (dotted line) in bulky microcrystalline powder excited at 355 nm by a Nd:YAG laser at room temperature. The emission around 1000 nm is assigned to the $^2F_{5/2} \rightarrow {}^2F_{7/2}$ transition of the Yb^{3+} ion. Since the absorption band of the Yb^{3+} ion ($^2F_{7/2} \rightarrow {}^2F_{5/2}$, ca. 980 nm) is beyond 355 nm, the excitation light is considered to be absorbed by HFA ligands in $Yb(HFA)_3$-$(TPPO)_2$ for the excitation wavelength brushes the absorption tail of the HFA ligands as shown in the inset of Figure 4a. The absorption of the TPPO ligands are blue-shifted relative to the HFA ligands and are excluded from the absorption of

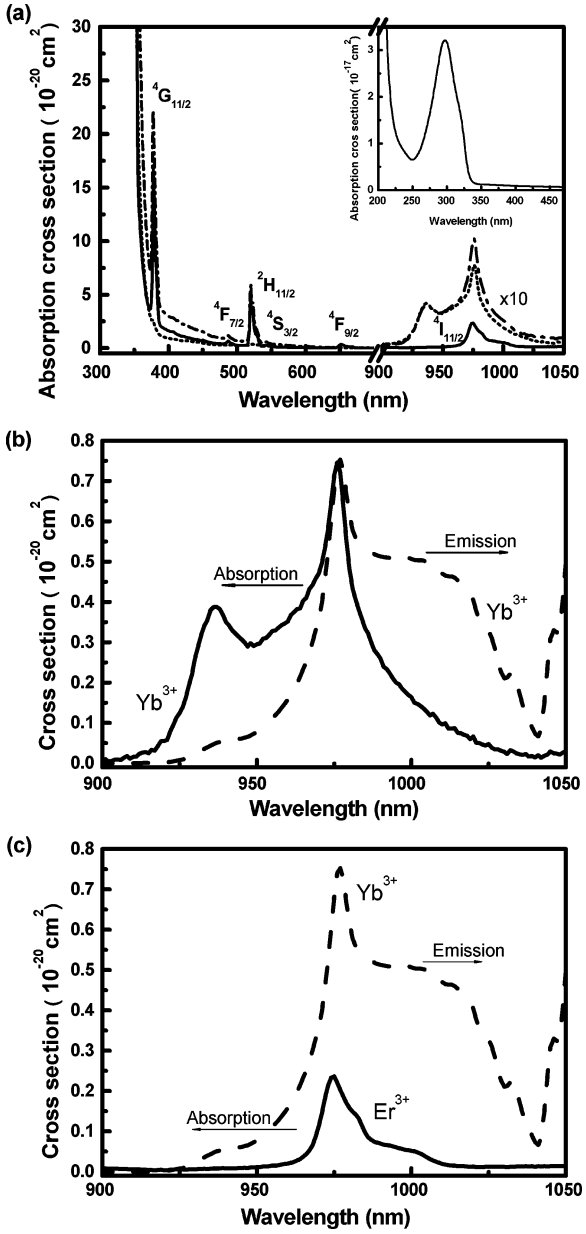

Figure 4. (a) UV−vis NIR absorption cross section spectra of $Er(HFA)_3$-$(TPPO)_2$ (solid line), $Yb(HFA)_3(TPPO)_2$ (dotted line), and $Er_{1/2}Yb_{1/2}$-$(HFA)_3(TPPO)_2$ (dashed line). The absorption bands at 900−1050 nm are magnified by 10-fold and lie on the superimposition of the $^4I_{15/2} \rightarrow {}^4I_{11/2}$ transition of $Er^{3+}$and the $^2F_{7/2} \rightarrow {}^2F_{5/2}$ transition of Yb^{3+}. The absorption bands in the erbium-related spectra correspond to transitions from the $^4I_{15/2}$ ground state to excited multiplet states. The inset is pointed toward the HFA ligand absorption in all complexes. Absorption cross-section spectra of (b) Yb^{3+} in $Er_{1/2}Yb_{1/2}(HFA)_3(TPPO)_2$ and (c) Er^{3+} in $Er_{1/2}Yb_{1/2}$-$(HFA)_3(TPPO)_2$. The emission cross-section spectra (calculated according to McCumber theory) of Yb^{3+} in $Er_{1/2}Yb_{1/2}(HFA)_3(TPPO)_2$ are shown in both panels b and c as dashed lines.

(11) Staveren, D. R. v.; Albada, G. A. v.; Haasnoot, J. G.; Kooijman, H.; Lanfredi, A. M. M.; Nieuwenhuizen, P. J.; Spek, A. L.; Ugozzoli, F.; ller, T. W.; Reedijk, J. *Inorg. Chim. Acta* **2001**, *315*, 163−171.
(12) Deacon, G. B.; Forsyth, C. M.; Gatehouse, B. M.; Philosof, A.; Skelton, B. W.; White, A. H.; White, P. A. *Aust. J. Chem.* **1997**, *50*, 959−970.
(13) Hebbink, G. A.; Reinhoudt, D. N.; Veggel, F. C. J. M. V. Eur. *J. Org. Chem.* **2001**, 4101−4106.

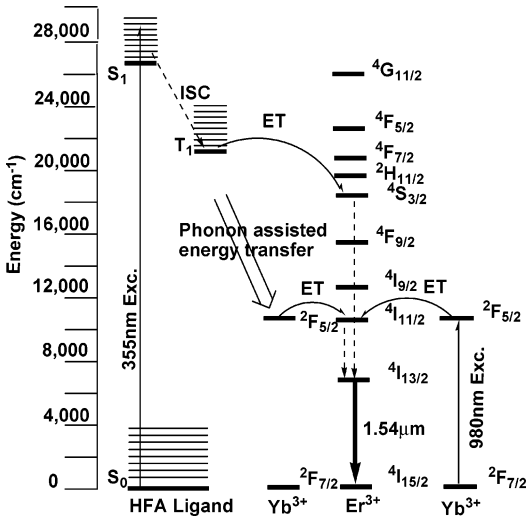

Figure 5. Schematic diagram for sensitization mechanism of the Er^{3+} ion by Yb^{3+} ion or HFA ligand.

355 nm excitation light. It might be possible that there is an energy transfer from the HFA ligands to Yb^{3+}, resulting in NIR PL of Yb^{3+} ion. However, the upper level $^2F_{5/2}$ of the Yb^{3+} ion is significantly low down to 10 200 cm^{-1}, which eliminates any possible energy match between the $^2F_{5/2}$ level and the HFA ligands' first singlet (S_1, ca. 26 000 cm^{-1}) or triplet level (T_1, ca. 22 200 cm^{-1}).[14] Therefore, the sensitization process may occur via a phonon-assisted energy transfer process (i.e., the nonradiative ($^2F_{7/2}-T_1$) → ($^2F_{5/2}-S_0$) process with the excess energy transformed into vibrational energy and ultimately heat as Güdel et al. proposed).[15]

Figure 3b shows the NIR PL spectrum of $Er(HFA)_3(TPPO)_2$ (dotted line) in bulky microcrystalline powder excited at 355 nm by an Nd:YAG laser at room temperature. The emission at around 1500 nm is assigned to the $^4I_{13/2} \rightarrow {}^4I_{15/2}$ transition of Er^{3+} ion. As indicated in Figure 5, the usual path for energy transfer from the HFA ligand to Er^{3+} ion involves $S_1 \rightarrow T_1$ intersystem crossing from singlet state, S_1, to triplet state, T_1, in the HFA ligand, which is enhanced by the coordinated heavy erbium ion,[16] and subsequent energy transfer from T_1 to energy levels of Er^{3+} ion. The enhanced intersystem crossing rate is interpreted in terms of an enhanced coupling between the singlet and triplet states or triplet and singlet ground states, respectively. In this case, indirect excitation on the Er^{3+} ion via the light absorption of the HFA ligands in $Er(HFA)_3(TPPO)_2$ is applicable because of the energy matching of the 4f levels of Er^{3+} such as $^4F_{5/2}$ (22 100 cm^{-1}), $^4F_{7/2}$ (20 400 cm^{-1}), and $^2H_{11/2}$ (19 100 cm^{-1}), with the triplet state (ca. 22 200 cm^{-1}) of the HFA ligands. In fact, such indirect excitation on the Tb^{3+} and Eu^{3+} ions via organic ligands has been well established when the energy of the triplet state of the ligand lies slightly above a potentially accepting energy level of the lanthanide ion. Since the energy gap between the $^4F_{5/2}$ level of the Er^{3+} and the triplet state of the HFA ligands is very small, about 100 cm^{-1}, the energy transfer efficiency will be limited because of the competitive energy back-transfer from the Er^{3+} ion to HFA ligand.[17,18] In terms of their corresponding energy gaps, the $^4F_{7/2}$ level might be the best accepting level of Er^{3+} in the complex.

According to Malta et al.,[19] the accepting lanthanide energy levels should obey the selection rules for energy-transfer. For the $^{2s+1}L_J$ levels of the lanthanide ion, the selection rules for energy transfer prescribe $|\Delta J| = 2, 4, 6$ for a multipolar mechanism (Förster mechanism) and $|\Delta J| = 0, 1$ ($J = J' \neq 0$) for an exchange mechanism (Dexter mechanism), respectively. Here ΔJ refers the difference of tthe momentum quanta for the accepting level and the ground level of lanthanide ion. $|\Delta J|$ is calculated to be equal to 4 for the energy transfer from the T_1 state of the HFA ligand to the $^4F_{7/2}$ level of Er^{3+}; therefore, such a $T_1 \rightarrow {}^4F_{7/2}$ energy transfer will follow Förster mechanism in complex $Er(HFA)_3(TPPO)_2$.

As shown in Figure 3b, the Er−Yb cocrystalline complex, $Er_{1/2}Yb_{1/2}(HFA)_3(TPPO)_2$, exhibits an enhanced luminescence intensity at 1500 nm for the Er^{3+} ion compared with monometallic complex $Er(HFA)_3(TPPO)_2$ because of the existence of Yb^{3+} in $Er_{1/2}Yb_{1/2}(HFA)_3(TPPO)_2$, while its luminescence intensity at 1000 nm for the Yb^{3+} ion decreases compared to that of monometallic complex $Yb(HFA)_3(TPPO)_2$ because of the Er^{3+} ion (Figure 3a). That is, the Yb^{3+} ion contributes to Er^{3+} ion's emission by delivering the energy from the HFA ligand to the Er^{3+} ion, for which the process is schematically sketched in Figure 5. Here, when the Er−Yb cocrystalline complex $Er_{1/2}Yb_{1/2}(HFA)_3(TPPO)_2$ is excited at 355 nm, the additional energy-transfer approach from the HFA ligand to Yb^{3+} ion via a phonon-assisted energy-transfer process and then the partial transfer to the Er^{3+} ion is the acceptable explanation for the enhancement on Er^{3+} ion's luminescence and the decrease of Yb^{3+} ion's luminescence in Figure 3.

Figure 6 gives the NIR PL spectrum of a bulky microcrystalline powder sample for $Er_{1/2}Yb_{1/2}(HFA)_3(TPPO)_2$ excited at 980 nm by a LD at room temperature with those of $Er(HFA)_3(TPPO)_2$ and $Yb(HFA)_3(TPPO)_2$ for comparison. The $Er_{1/2}Yb_{1/2}(HFA)_3(TPPO)_2$ exhibits markedly enhanced luminescence intensity compared with that of $Er(HFA)_3(TPPO)_2$ around 1500 nm and significantly decreased luminescence intensity compared with that of $Yb(HFA)_3(TPPO)_2$ around 1000 nm. This, combined with the fact that Yb^{3+} has 1 order of magnitude greater absorption cross-section than Er^{3+} in a 980 nm band, as shown in Figure 4a,

(14) Sager, W. F.; Filipescu, N.; Serafin, F. A. *J. Phys. Chem.* **1965**, *69*, 1092−1100.
(15) Reinhard, C.; Güdel, H. U. *Inorg. Chem.* **2002**, *41*, 1048−1055.
(16) (a) Guldi, D. M.; Mody, T. D.; Gerasimchuk, N. N.; Magda, D.; Sessler, J. L. *J. Am. Chem. Soc.* **2000**, *122*, 8289−8298. (b) Tobita, S.; Arakawa, M.; Tanaka, I. *J. Phys. Chem.* **1985**, *89*, 5649−5654. (c) Tobita, S.; Arakawa, M.; Tanaka, I. *J. Phys. Chem.* **1984**, *88*, 2697−2702.
(17) Sato, S.; Wada, M. *Bull. Chem. Soc. Jpn.* **1970**, *43*, 1955−1960.
(18) Latva, M.; Takalo, H.; Mukkala, V.-M.; Matachescu, C.; Rodríguez-Ubis, J. C.; Kankare, J. *J. Lumin.* **1997**, *75*, 149−169.
(19) (a) Malta, O. L. *J. Lumin.* **1997**, *71*, 229−236. (b) Goncüalves e Silva, F. R.; Malta, O. L. *J. Alloys Compd.* **1997**, *250*, 427−430. (c) Malta, O. L.; Goncüalves e Silva, F. R. *Spectrochim. Acta A* **1998**, *54*, 1593−1599. (d) de Sá, G. F.; Malta, O. L.; de Mello Donegá, C.; Simas, A. M.; Longo, R. L.; Santa-Cruz, P. A.; da Silva, E. F., Jr. *Coord. Chem. Rev.* **2000**, *196*, 165−195.

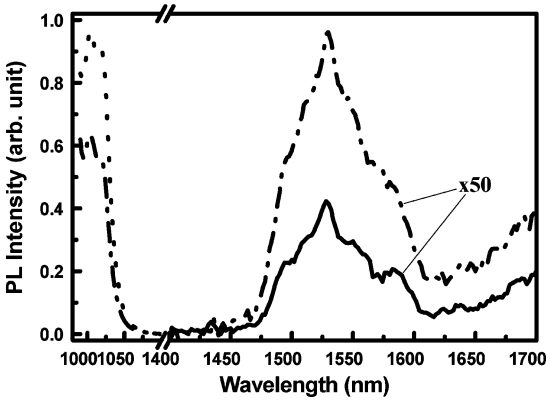

Figure 6. NIR PL spectra of bulky microcrystalline powder samples of $Er(HFA)_3(TPPO)_2$ (solid line), $Er_{1/2}Yb_{1/2}(HFA)_3(TPPO)_2$ (dashed line), and $Yb(HFA)_3(TPPO)_2$ (dotted line) excited at 980 nm. PL curves at around 1500 nm are magnified by 50-fold.

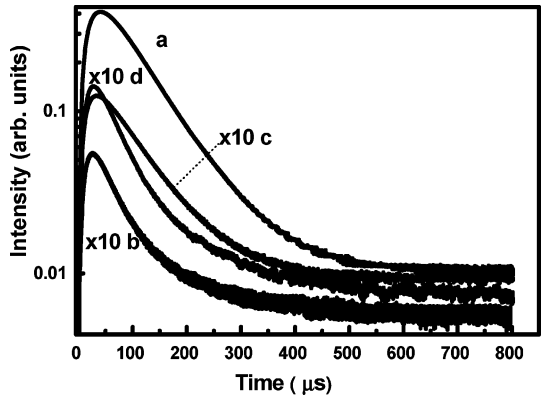

Figure 7. Time dependence for the luminescence of the $^2F_{5/2}$ level of Yb^{3+} in $Yb(HFA)_3(TPPO)_2$ microcrystalline powder monitored at 1020 nm (a). Time dependence for the luminescence of $^4I_{13/2}$ level of Er^{3+} in $Er(HFA)_3(TPPO)_2$ microcrystalline powder monitored at 1530 nm (b). Time dependence for the luminescence of Yb^{3+} (c) and Er^{3+} (d) in $Er_{1/2}Yb_{1/2}(HFA)_3(TPPO)_2$ microcrystalline powder. The photoluminescence for all is under excitation with a 10 ns pulse at 355 nm.

shows that Yb^{3+} indeed contributes to the enhancement in the luminescence intensity of Er^{3+} for $Er_{1/2}Yb_{1/2}(HFA)_3(TPPO)_2$. As shown in Figure 5, the $^4I_{11/2}$ level of the Er^{3+} ion is excited indirectly via effective energy transfer from the $^2F_{5/2}$ level of theYb^{3+} ion to it, and it subsequently decays to a lower level, $^4I_{13/2}$, which finally results in NIR emission of the Er^{3+} ion's $^4I_{13/2} \rightarrow {}^4I_{15/2}$ transition.

Energy-Transfer Quantum Efficiency and Identification of Yb−Er Energy-Transfer Mechanism. The time-dependent NIR luminescence spectra of Yb^{3+} ion originating from $^2F_{5/2}$ level and Er^{3+} ion originating from $^4I_{13/2}$ level in $Er_{1/2}Yb_{1/2}(HFA)_3(TPPO)_2$ microcrystalline powder, upon excitation with a 10 ns pulse at 355 nm, are in shown Figure 7b and c which are monitored at 1020 and 1530 nm, respectively. For comparison, the time-dependent NIR luminescence spectra for the monometallic complexes, $Yb(HFA)_3(TPPO)_2$ and $Er(HFA)_3(TPPO)_2$, are presented in Figure 7a and b. As the luminescence and its decay curve from the $^4I_{11/2}$ level of the Er^{3+} ion are not detectable because it is quickly nonradiatively de-excited to the $^4I_{13/2}$ level because of the high vibration mode of C−H groups, the luminescence lifetimes for Er^{3+} and Yb^{3+} can be monoexponentially fitted from the declining parts of the luminescence decay curves. The lifetimes for Yb^{3+} in monometallic $Yb(HFA)_3(TPPO)_2$ and Er−Yb cocrystalline complex $Er_{1/2}Yb_{1/2}(HFA)_3(TPPO)_2$ are 89.1 and 83.7 μs, respectively, while those for Er^{3+} in monometallic $Er(HFA)_3(TPPO)_2$ and Er−Yb cocrystalline complex $Er_{1/2}Yb_{1/2}(HFA)_3(TPPO)_2$ are 60.8 and 61.0 μs, respectively. On the basis of their corresponding pure radiative lifetimes of 2 and 14 ms for Yb^{3+} and Er^{3+}, respectively,[20] the quantum yields for Yb^{3+} in monometallic $Yb(HFA)_3(TPPO)_2$ and Er−Yb cocrystalline complex $Er_{1/2}Yb_{1/2}(HFA)_3(TPPO)_2$ are 4.46×10^{-2} and 4.19×10^{-2}, respectively, while those for Er^{3+} in monometallic $Er(HFA)_3(TPPO)_2$ and Er−Yb cocrystalline complex $Er_{1/2}Yb_{1/2}(HFA)_3(TPPO)_2$ are 4.34×10^{-3} and 4.36×10^{-3}, respectively. Such low luminescence efficiencies, particularly for Er^{3+}, are attributed to the luminescence quenching by a number of C−H groups, as described earlier in this work. The luminescence lifetime and quantum yield for Er^{3+} remain nearly constant, comparing $Er(HFA)_3(TPPO)_2$ with $Er_{1/2}Yb_{1/2}(HFA)_3(TPPO)_2$, while those for Yb^{3+} decrease a little, comparing $Yb(HFA)_3(TPPO)_2$ with $Er_{1/2}Yb_{1/2}(HFA)_3(TPPO)_2$, which can be understood as a consequence of the additional de-excitation channel for Yb^{3+} resulting from the Yb−Er energy transfer. In view of the remarkable enhancement in Er^{3+} luminescence intensity by Yb^{3+}, as previously mentioned, only a small decrease in the lifetime of Yb^{3+} is observed, and this may be caused by the effect of irradiative energy transfer among the Yb^{3+} ions simultaneously.

As shown in Figure 7, the decay curves exhibit a remarkable rising trend in the beginning. The monoexponentially increasing time-constant of 9.4 μs for Er^{3+} in $Er(HFA)_3(TPPO)_2$ is comparable to the lifetime of radiative decay for HFA ligand's triplet state at 77 K.[21] Whene energy transfer from the HFA ligand triplet state to the Er^{3+} ion is in progress, generally the lanthanide luminescence intensity is expected to increase with a rate equal to the decay rate of the ligand's triplet state at 77 K during this process. This demonstrates that the pathway of sensitized emission upon UV excitation indeed involves the triplet state of the HFA ligand. The increasing time constant of 12.7 μs for the Yb^{3+} in $Yb(HFA)_3(TPPO)_2$ may be considered to be the time constant for the phonon-assisted energy transfer from the HFA ligand to the Yb^{3+} ion, which is a little larger than that for energy transfer originating from the HFA ligand's triplet state to the Er^{3+} ion. It is deduced that the energy transfer originating from the ligand's triplet state to the Er^{3+} ion is a little faster than the phonon-assisted energy transfer between the ligand and the Yb^{3+} ion. In the meantime, the time constant of 10.6 μs for the Yb^{3+} in $Er_{1/2}Yb_{1/2}(HFA)_3(TPPO)_2$ decreases in comparison to that of 12.7 μs for the Yb^{3+} in $Yb(HFA)_3(TPPO)_2$, while the time constant of 11.3 μs for Er^{3+} in $Er_{1/2}Yb_{1/2}(HFA)_3(TPPO)_2$ increases in comparison to that of 9.4 μs for Er^{3+} in $Er(HFA)_3(TPPO)_2$. There should be an interactive energy transfer between Yb^{3+}

(20) Klink, S. I.; Hebbink, G. A.; Grave, L.; Peters, F. G. A.; Veggel, F. C. J. M. V.; Reinhoudt, D. N.; Hofstraat, J. W. *Eur. J. Org. Chem.* **2000**, 1923−1931.
(21) Freeman, J. J.; Crosby, G. A. *J. Phys. Chem.* **1963**, *67*, 2717−2723.

and Er^{3+} that may moderate the time-constant difference between Yb^{3+} and Er^{3+}.

The quantum efficiency, η, of the energy transfer from Yb^{3+} to Er^{3+} in Er−Yb cocrystalline complex $Er_{1/2}Yb_{1/2}(HFA)_3(TPPO)_2$ is approximately defined from the formula

$$\eta_\tau = 1 - \tau_{Yb,Er}/\tau_{Yb} \quad (1)$$

where τ_{Yb} and $\tau_{Yb,Er}$ are the lifetimes for the Yb^{3+} luminescence intensity in monometallic $Yb(HFA)_3(TPPO)_2$ and Er−Yb cocrystalline complex $Er_{1/2}Yb_{1/2}(HFA)_3(TPPO)_2$, respectively. The decrease of the Yb^{3+} lifetimes for the two species corresponds to 6.06% efficiency for Yb−Er energy transfer.

Since six representative Yb···Er distances in Er−Yb cocrystalline complex $Er_{1/2}Yb_{1/2}(HFA)_3(TPPO)_2$ crystal are larger than 10 Å, as deduced from the molecular packing of $Er(HFA)_3(TPPO)_2$, as mentioned above, it should be hypothetically assumed that the intermolecular energy transfer should be modeled by the Förster mechanism based on an electric dipole−dipole interaction rather than the Dexter mechanism.[22] An excitation caused by the optical absorption of a donor ion (here, the Yb^{3+} ion) can be transferred to an nearby acceptor ion (here, the Er^{3+} ion) or another nearby donor ion as the dipole−dipole interaction for the energy-transfer process is operative. On the basis of the McCumber theory and Förster model, the distances between Er^{3+} and Yb^{3+} ions can be determined by analysis of the luminescence decay of the donor and then calculated from the energy-transfer efficiency, which is verified with the data obtained from the crystallographic measurement. The modeling process is mainly composed of three steps with the details in the Supporting Information. First, Figure 4b presents the emission cross-section spectrum of the $^2F_{5/2}$ level of Yb^{3+} ion, calculated according to McCumber theory.[23] The spectral overlap between the emission cross-section spectrum of the Yb^{3+} ion and the absorption cross-section spectrum of the Er^{3+} ion in $Er_{1/2}Yb_{1/2}(HFA)_3(TPPO)_2$ is shown in Figure 4c. Second, the donor−donor (here, the donor is the Yb^{3+} ion) energy-transfer critical radius, $R_{C,DD}$, and donor−acceptor (here, the acceptor is the Er^{3+} ion) energy-transfer critical radius, $R_{C,DA}$, are calculated to be 9.46 and 7.44 Å, respectively, by the overlap integral method which is based on the calculation of the donor emission and the acceptor or donor absorption cross-section superimposition.[24] Finally, the quantum efficiency of energy transfer is evaluated using the equation[25]

$$\eta_{R_C} = (1 + (r/R_C)^6)^{-1} \quad (2)$$

Here, the quantum efficiency of energy transfer for Yb^{3+} obtained from $R_{C,DA}$ is equal to that from τ_D. Thus, the estimated Er···Yb distance, r, is calculated to be 11.75 Å from the $R_{C,DA}$ value, which matches reasonably well with the average value of 11.99 Å of those distances obtained from molecular packing in Er−Yb cocrystalline complex $Er_{1/2}Yb_{1/2}(HFA)_3(TPPO)_2$.

Conclusion

In summary, the novel Er−Yb cocrystalline complex $Er_{1/2}Yb_{1/2}(HFA)_3(TPPO)_2$ exhibits sensitized NIR emission with luminescence lifetimes in the microsecond range. The intermolecular energy transfer is modeled by the Förster mechanism, based on an electric dipole−dipole interaction. The critical radii for energy transfer obtained from the fits to this model are estimated with the donor−donor energy-transfer critical radius, $R_{C,DD}$, and donor−acceptor energy-transfer critical radius, $R_{C,DA}$, values of 9.46 and 7.44 Å, respectively.

Acknowledgment. The authors would like to thank Gu Jianmin for the X-ray analysis of the single-crystal samples. The authors also gratefully acknowledge the financial support for this work from the National Natural Science Foundation of P. R. China (No. 50532030) and the Foundation for the Author of National Excellent Doctoral Dissertation of P. R. China (No. 200134). The authors are grateful for the referees' helpful suggestions.

Supporting Information Available: Listing of FTIR spectra of all complexes referred in the article and EDS analysis for the complexes $Er_{1/2}Yb_{1/2}(HFA)_3(TPPO)_2$, crystallographic data in CIF format, DSC diagrams of the complexes $Er(HFA)_3(TPPO)_2$, $Yb(HFA)_3(TPPO)_2$, $Er_{1/2}Yb_{1/2}(HFA)_3(TPPO)_2$, and the mechanical mixture of $Er(HFA)_3(TPPO)_2$ and $Yb(HFA)_3(TPPO)_2$ (molar ratio of 1:1), TG diagram of the complex $Er_{1/2}Yb_{1/2}(HFA)_3(TPPO)_2$, and a detail discussion of the verification process of the Yb−Er energy-transfer mechanism. This material is available free of charge via the Internet at http://pubs.acs.org.

IC051697Y

(22) (a) Dexter, D. L. *J. Chem. Phys.* **1952**, *21*, 836−850. (b) Froidevaux, P.; Biinzli, J.-C. G. *J. Phys. Chem.* **1994**, *98*, 532−536. (c) Klink, S. I.; Grave, L.; Reinhoudt, D. N.; Veggel, F. C. J. M. v.; Werts, M. H. V.; Geurts, F. A. J.; Hofstraat, J. W. *J. Phys. Chem. A* **2000**, *104*, 5457−5468.

(23) McCumber, D. E. *Phys. Rev. B* **1964**, *136*, A954−957.

(24) Tarelho, L. V. G.; Gomes, L.; Ranieri, I. M. *Phys. Rev. B* **1997**, *56*, 56−63.

(25) (a) Ajithkumar, G.; Unnikrishnan, N. V. *Solid State Comm.* **1997**, *104*, 29−33. (b) Horrocks, W. D. J.; Rhee, M.-J.; Snyder, A. P.; Sudnick, D. R. *J. Am. Chem. Soc.* **1980**, *102*, 3650−3652.